Experimental Study on the Mean Flow Characteristics of Forward-Curved Centrifugal Fans

Eui-Yong Kwon, Nam-Hyo Cho*

Institute for Advanced Engineering Yongin, P. O. Box 25, Kyonggi-do, 449-863, Korea

Measurements have been made in an automotive HVAC blower for two different centrifugal fans. This work is directed at improving the performance of a conventional forward-curved centrifugal fan for a given small blower casing. Mean velocities and pressure have been measured using a miniature five-hole probe and a pressure scanning unit connected to an online data acquisition system. First, we obtained the fan performance curves versus flow rates showing a significant attenuation of unstable nature achieved with the new fan rotor in the surging operation range. Second, aerodynamic characterizations were carried out by investigating the velocity and pressure fields in the casing flow passage for different fan operating conditions. The measurements showed that performance coefficients are strongly influenced by flow characteristics at the throat region. The main flow features were common in both fans, but improved performance is achieved with the new fan rotor, particularly in lower flow rate regions. Based on the measured results, design improvements were carried out in an acceptable operation range, which gave considerable insight into what features of flow behavior were most important.

Key Words : HVAC Blower, Forward-Curved Centrifugal Fan, 5 Hole Probe, Flow Measurements, Vortex

Nomenclature

b : Rotor width
B : Casing width
c : Blade chord length
C : Cut-off clearance
C_p : Pressure coefficient for calibration
C_{pw} : Casing wall pressure coefficient
C_T : Reference pressure coefficient for data validation
C_V : Velocity coefficient for calibration
D_0 : Casing inlet opening diameter
D_1, D_2 : Rotor inlet and outlet diameter
N : Number of blades
p : Static pressure
p_t : Total pressure
P_{shaft} : Rotor shaft power
q : Dynamic pressure
Q : Volume flow rate
r, θ_s, Z : Cylindrical coordinates (Fig. 1)
R_s : Scroll radius
Re : Reynolds number
S : Blade pitch
U : Blade speed
V : Flow velocity
α_s : Scroll angle
β : Blade angle
η : Total fan efficiency
φ : Nondimensional flow coefficient
ν : Kinematic viscosity
ρ : Density
ψ : Nondimensional total pressure coefficient

Subscripts

1, 2 : Rotor inlet, outlet or blade tip
1, 2, 3, 4, 5 : Holes of five hole probe (Fig. 3)
amb. ref : Ambient, reference conditions

* Corresponding Author,
E-mail : nhcho@iae.re.kr
TEL : +82-31-330-7415; **FAX** : +82-31-330-7116
Institute for Advanced Engineering, Yongin P. O. Box 25, Kyonggi-do, 449-863, Republic of Korea. (Manuscript **Received** June 5, 2001; **Revised** September 1, 2001)

av, max: Average, maximum
C, R : Casing, rotor
e, i : Entrance, inlet locations of pressure probe (Fig. 10)
r, t : Radial, tangential velocity components

1. Introduction

Current automotive HVAC (heating, ventilating and air-conditioning) system is to make the products more powerful, efficient, smaller, and preferably quieter. Among various types of fan rotors used in HVAC systems, FC (forward-curved) fan is the most widely used due to its low cost and its capacity to deliver a large quantity of air and hence, higher pressure rise. The quality and quantity of the airflow and noise from the products must be considered to make sure that its system operates properly before mass production. Modern design has tended to lead to the use of a smaller HVAC system to satisfy various automobile functions demands. This leads to a relatively more complicated air handling problem and therefore complex design requirements, the needs for increased performance, all leading to greater aero-acoustic problems. To cope with the increasing demand for higher performance and lower noise in small HVAC blowers, the rotor is usually designed and fitted around a given blower casing. For this purpose many investigations have been made with special attention to aero-acoustical performance. Morinushi (1987) and Roth (1981) determined some major geometric parameters for designing low noise FC centrifugal fans. Bommes et al. (1995) and Fehse and Neise (1999) characterized the low-frequency noise induced by flow separation in blade channels and the casing passages, resulting in higher turbulence intensities. Shepherd and Lafontaine (1992) addressed the noise generated by unsteady loading on the rotor due to separated flows. The characterization of high frequency noise (i.e. tonal noise), has been done by many investigations (Koopmann et al., 1988, Ohta et al. , 1996, Velarde-Suarez et al., 1999). This aerodynamic noise is known to be generated by pressure fluctuations within the vicinity of the cut-off, which is in turn produced by the flow leaving the blade channels.

Whereas there have been a number of experimental papers on fan rotor centrifugal fans a few of them has been focused on design improvement. Rotor exit velocities were measured by Raj and Swim (1981) and Cau et al. (1987) by using a hot-wire probes. Useful results about reverse flow through rotor blades and the presence of rotor losses, have been obtained by Kind and Tobin (1990) from detailed measurements of the mean flow-field for three different blower configurations by using a five-hole probe. However, we need more information on the casing passage flow, such as the development of the vortex flow and gradients both in spanwise and radial directions downstream of the cut-off. Through this we can understand the aerodynamic flow features and improvement rotor design.

The aim of the present study is to present the pressure and three mean velocity data measured in the casing passage to describe the fundamental flow characteristics of FC centrifugal fans. This can lead to a deeper understanding of flow structures and, hence, to improved fan performance by extending the flow analysis to incorporate the rotor shape effect. Flow-field measurements are carried out for two different rotors with the same blower casing at three operating conditions. First, fan performance curves and pressures on the casing surface are obtained. Second, velocity field in various circumferential locations of the casing passage is investigated.

2. Experimental Apparatus and Method

2.1 Fan dimensions

The fan selected for this study was a single inlet FC centrifugal fan with a squirrel cage rotor. To study the effect of the rotor shape in the same blower casing, two FC rotors (model Ⅰ & Ⅱ) were constructed with the same outer diameter but different blade shapes. Nomenclature for the blade shapes and the fan is given in Fig. 1. The basic blade shapes of Model I & II were both a

Table 1 Parameters of the tested fan configurations

		Model Ⅰ	Model Ⅱ
Rotor			
Fan inlet diameter	D_1(mm)	116	109
Fan outlet diameter	D_2(mm)	140	140
Fan width	b(mm)	65	68.2
Number of blades	N	44	41
Inlet blade angle	β_1(deg)	15	0
Outlet blade angle	β_2(deg)	−66	−66
Blade chord length	c(mm)	13.5	18.6
Pitch to chord ratio	S/c(%)	73.3	55.4
Blower casing			
Casing width	B(mm)	84	←
Cut-off clearance	C(mm)	11.8	←
Scroll angle at θ_s=210°	α_s(deg)	5	←
Diameter of inlet opening	D_0(mm)	112.7	←

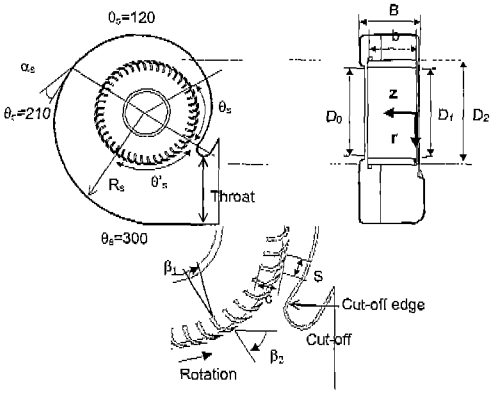

Fig. 1 Diagram of the FC centrifugal fan

circular arc-type but with different inlet blade angle, camber radius, exit-to-inlet area ratio, and pitch-to-chord ratio. Their specifications are given in Table 1. The blade shape of Model II is defined from a one dimensional design code, which uses a method based on superposition of sources and vortices. Previously, one dimensional performance analysis has been made for various design blade parameters such as thickness-to-chord ratio, camber, leading edge and trailing edge radius and so on. The results showed significant difference in lift, drag and moment coefficient. These aerodynamic parameters are useful in predicting the pressure rise and the flow stability versus volume flow rate of the fan.

Both fans had the same casing; see Table 1. The

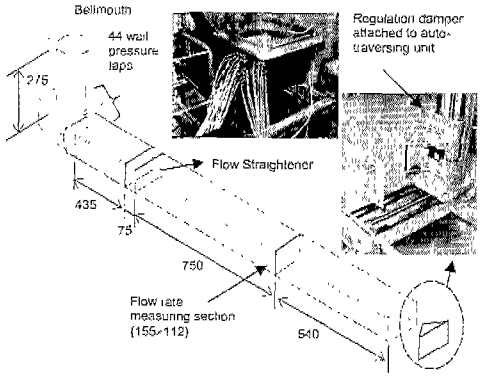

Fig. 2 Fan test apparatus

cross sectional area of the blower casing was increased with the scroll angle in the following logarithmic law, starting from the origin (i.e. cut-off edge) to θ_s=300deg :

$$R_s=\frac{D_2}{2}\exp\left\{(\theta_s+\theta_s')\tan\frac{\pi}{30}\right\} \quad (1)$$

The casing had a rather large clearance of 11.8mm between the cut-off and the blade tips.

2.2 Measurement

The system diagram and the main specifications of the fan test apparatus are shown in Fig. 2. The test apparatus and the aerodynamic performance measurement were made according to the ANSI/AMCA Standard 210-85. The inlet bellmouth duct was straight and free of obstruction. After leaving the fan, air passes through a straightener to remove swirl and generate a uniform flow. At the end of the outlet duct a regulation damper, which is clamped to a traversing mechanism, controls the fan operating point. The volume flow rate is measured by an averaging Pitot tube, static pressure taps and a thermocouple. The total pressure rise across the fan is determined by adding dynamic pressure to the static pressure measured in the outlet duct. The test fan is driven by a 30V/30A regulated DC power supply. Its rotational speed is measured with an optical fiber sensor connected to a digital RPM indicator. All flow parameters except the fan RPM are measured and displayed in real time from online data acquisition system controlled by LabVIEW®. The 12-bit A/D conversion is done at a frequency

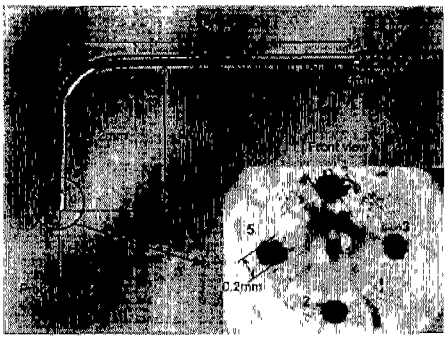

Fig. 3 Five hole probe

of 100kHz, and the step motor is controlled done by a digital I/O interface which operates at 32bits.

Surface pressures on the blower casing are measured by a pressure scanning system with 24 port valves (Scanivalve®) connected to a Setra ± 63 mmH_2O differential transducer. Moreover, a miniature five-hole probe of 2 mm outer diameter is used to measure velocity. The probe had a conical head with pressure taps of 0.2 mm diameter (Fig. 3). In use, the probe axis was always perpendicular to the radial axis of the fan rotor. Special care was paid to the calibration procedure and data processing in order to extend the validity of measured angles up to ±55 deg. For low-angle regime the calibration grid in angle was half that of large-angle regime in order to take into account the strong nonlinear gradients at the surface of the probe's head, i.e. $\Delta=3$ deg in the range ± 21 deg instead of $\Delta=6$ deg for higher angles. During calibration, the angle coefficients $C_\alpha=(p_3-p_5)/(p_1-p_{av})$ and $C_\beta=(p_4-p_2)/(p_1-p_{av})$ are determined for all calibration angles α and β. In real use, these angles are first determined then, the static and dynamic pressure of the flow are deduced from interpolation referring to the calibration map defined by the velocity and pressure coefficients, i.e. $C_V=(p_1-p_{av})/q$ and $C_p=(p-p_1)/(p_1-p_{av})$ with $q=\rho V^2/2$. The calibration coefficients are calculated by the average pressure $p_{av}=\Sigma(p_2, p_3, p_4, p_5)/4$ and $p_{av}=$minimum(p_2, p_3, p_4, p_5) for low and high-angle regimes, respectively. Thus, the coefficients depend only on the value of p_1 and not on intermediate calculations, reducing the risk of error. The measurement error of the probe can be firstly deduced from the calibration map but in a complex flow-field where swirling flow occurs this error increases substantially. It is found that for the velocity in the range 10-40 ms^{-1}, the measurement error remained of the order of ±1 deg in angles, ±1% in the tangential velocity component and ±3% in radial and axial velocity components. These errors include uncertainties due to pneumatic effect and A/D conversion. In order to reject acquisition points for which the flow inclination angle is too large to be processed, a pressure coefficient $C_T=(p_{max}-p_1)/(p_{max}-p_{av})$, which is independent of all intermediate calculation and the static and dynamic pressures of the flow, is used as a criterion. Here the average pressure p_{av} is defined as the same one used in low-angle regime. Prior investigations performed in a calibration bench as well as measurements in a wind-tunnel at the Aerodynamic Research Laboratory. (LEA) of the University of Poitiers in France have shown that this criterion remained valid in both in the region of reverse flow and high shear flow such as the wake. In the present study all the acquisition points for which the value of C_T exceeds $C_T=0.9$ are rejected in data processing. Repeatability of the measured data is addressed on the mounting effect of the model and on the day-to-day changes in ambient conditions. These uncertainties are accounted for by a complete reassembly of the blower module and by correction and the use of reference pressure. The variation in pressure rise across the fan is found to be of the order of ±1%.

3. Results and Discussions

3.1 Aerodynamic fan performance curves

Performance curves for the two tested fans are shown in Fig. 4. In this paper, all flow parameters are non-dimensional, as defined in Table 2. Model I, a model of the original commercial fan, gave a peak efficiency of 0.47. Its curves show a typical behavior of FC blade centrifugal fan. Here, the fan efficiency η is determined by the electric power of the drive motor supplied by the

Table 2 Aerodynamic non-dimensional parameters

Parameter	Formulation	Normalized value
Flow coefficient (φ)	$\varphi=\frac{4Q}{\pi D_2^2 U_2}$	$Q'=\pi D_2^2 U_2/4$
Total pressure coefficient (ψ)	$\psi=\frac{2\Delta p_t}{\rho_{ref} U_2^2}$	$p'=0.5\rho_{ref}U_2^2$
Total-to-total fan efficiency (η)	$\eta=\frac{Q\Delta p_t}{P_{shaft}}$	$P'=P_{shaft}$ =Torque×W =Torque×RPM×2 $\pi/60$

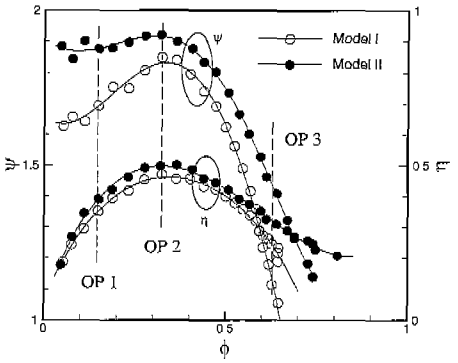

Fig. 4 Fan performance curves

manufacturer. As seen in Fig. 4, the highest total pressure and the best efficiency data are obtained with Model II. Its peak pressure and efficiency, at $\varphi=0.32$, are 5% and 7% higher than Model I, respectively. Model II produces higher flow rates than Model I for a given pressure at $\varphi\geq 0.45$. Particularly in the low flow rate region, (i.e. $\varphi\leq 0.3$), a high pressure rise (i.e. increase of aerodynamic performance) is achieved with Model II resulting in less steep positive slope. The generation of aerodynamic unstable phenomena in this low flow rate region would be attenuated significantly compared to Model I, since flow instabilities caused by separated flow in the blade passage and reverse flow are known to the decrease aerodynamic performance and increase noise (Cau et al., 1987). In spite of the large differences in blade design, both fans had their BEP (best efficiency point) at a flow coefficient near 0.32.

Another representation of fan performance is given in Fig. 5. It shows the variation of Reynolds numbers, Re_C and Re_R, with respect to flow

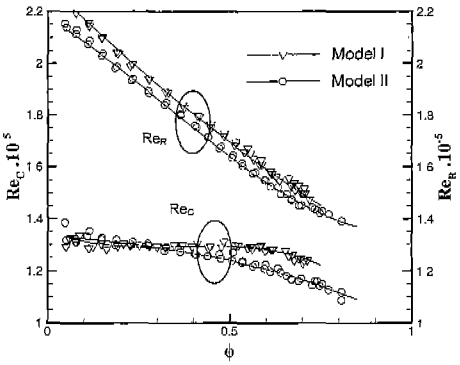

Fig. 5 Relation between characteristic Reynolds numbers and flow coefficient

coefficient. The Values of $Re_C(=U_{ref}D_{ref}/\nu$ at the flow rate measuring section) and $Re_R(=U_2D_2/\nu)$ are derived from characteristic velocity and diameter that illustrate the flow behavior of the scroll casing and the rotor, respectively. Unlike Re_C, Re_R decreases steeply and almost linearly with increasing flow rate. Hence we observe a large difference between the two Reynolds numbers at low flow rates, which gradually decreases with increasing flow rate. This behavior illustrates the important role of the rotor and the blower casing in fan performance. For flow rates below BEP, the rotor has a major influence on aerodynamic performance. At flow rates above BEP, the role of the casing becomes substantially important. Thus, for any given rotor, the sudden pressure drop at high flow rate (c.f. Fig. 4) can be avoided mainly by improving the casing design.

3.2 Pressure measurements on the casing

44 pressure taps of 0.3mm diameter were placed on the scroll casing at circumferential locations between $\theta_s=8.3$ and 57.5 deg. Surface pressure distributions for three different flow rates and the location of the pressure taps on the scroll casing are shown in Fig. 6. These operating points-designated as OP1, OP2 (BEP), and OP3-correspond to $\varphi=0.15$, 0.32 and 0.63, respectively, and are shown in Fig. 3. Results are represented in pressure coefficient, $C_{pw}=2(p_w-p_{amb})/(\rho_{amb}U_2^2)$, form. The non-dimensional pressure coefficient calculated from ambient flow conditions (p_{amb}, T_{amb}) and rotor tip velocity (U_2) allow us to

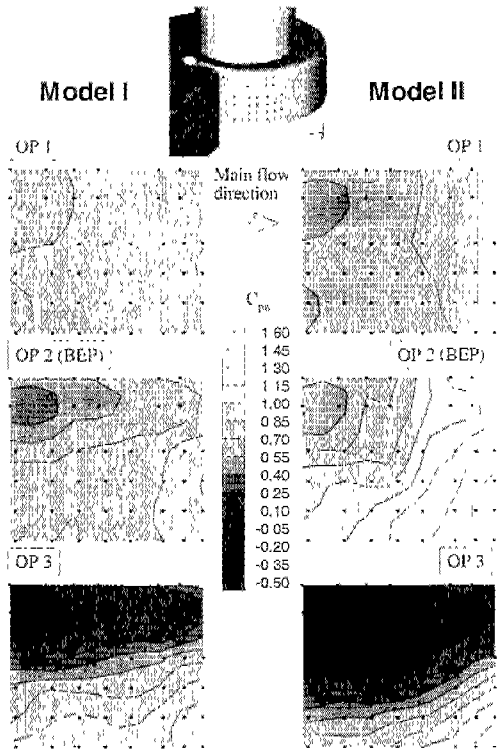

Fig. 6 Distributions of static pressure coefficient on the scroll casing at three operating points

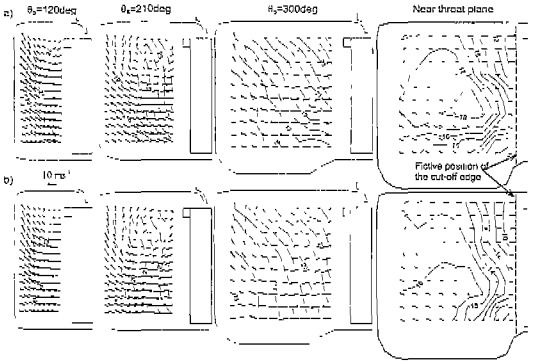

Fig. 7 Velocity vectors and iso-value contours of the streamwise velocity at various circumferential sections, at OP 2; (a) Model Ⅰ and (b) Model Ⅱ

examine the influence of rotor shape regardless of its rotational speed and changes in atmospheric conditions. As seen in Fig. 6, the flow exhibits generally similar behavior in both fan configurations. Flow behavior is, however, distinctly dependent on the operating conditions of the fans. As the flow rate increases, the overpressure region ($C_{pw} \geq 0$) appearing on the lower portion of the casing becomes more pronounced in both magnitude and in size. This is accompanied by an increase in pressure gradient in the direction of the rotation axis. This phenomenon was not unexpected since a higher flow rate is always associated with higher rotor exit velocity. Usually radial velocity component increases gradually with increasing flow rate, whereas tangential velocity component remains relatively constant. Therefore, in the high flow region above BEP ($\varphi > 0.32$), the casing obstructs the flow leaving the rotor exit, and consequently the blockage effect becomes more important. This blockage effect is directly related to energy loss, which means the velocity energy generated by the rotor does not transform effectively in pressure energy. The comparative data of Models I & II show similar flow behavior except that Model II reveals a much lower pressure level, particularly at OP1 and OP3. This fact can be attributed to better flow guidance and consequently a stronger "scooping" effect of Model II FC blade where the outlet air velocity at the trailing edge appears greater than the blade tip velocity. Lower pitch-chord ratio (S/c) and higher camber radius (i.e. strongly forward-facing at rotor exit) of Model II are assumed to be the principal parameters affecting this effect (Morinushi, 1987, Eck, 1973, Kind, 1997). This is, of course, consistent with the trend observed in fan performance curves, i.e. increase of total pressure rise across the fan (c.f. Fig. 4).

3.3 Velocity measurements in the casing

Figure 7 shows flow velocities in the casing passage at three circumferential sections, θ_s=120, 210 and 300deg, and a cross-section 8mm ahead of the cut-off edge at OP 2. To minimize the probe blockage effect, a distance bigger than 5mm was kept between the casing surface and the measurement points. Over this range the variation in total pressure was ±0.5 %. In both models the general flow behavior remains the same as it

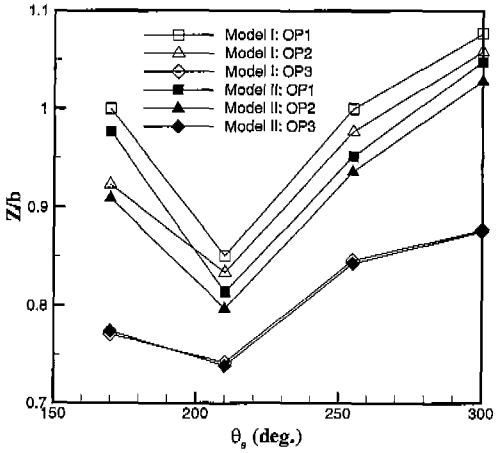

Fig. 8 Axial positions of the vortex core

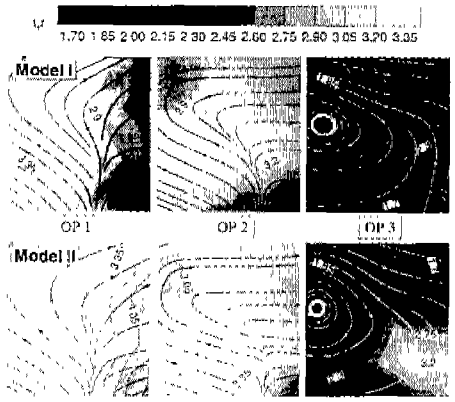

Fig. 9 Streamlines and distributions of total pressure coefficient on the throat plane

flows from upstream of the cut-off to a location near the throat of the casing. As expected, the magnitude of the streamwise velocity is large compared with other velocity components, given that the tangential and the radial component of the flow exiting the rotor are both large with the tangential component being dominant. The overall magnitude of the streamwise velocity and the location of its highest value do not change significantly as the flow progresses through the casing passage, except near the throat plane where the magnitude decreases to U=10 ms^{-1} and the region of highest value moves approximately to the middle of the plane. While no vortex flow is evident in the upstream location (θ_s=120 deg), it can be seen at downstream locations, θ_s=210 and 300 deg. The vortex core changes its position with respect to the circumferential location. As illustrated in Fig. 8, a vortex flow appears in all flow operating conditions between θ_s=170 and 300 deg. Both models show almost the same evolution; the axial position of the vortex core is the lowest at θ_s=210 deg and gradually moves towards the front plate of the casing.

While the flow pattern at the downstream locations up to θ_s=300 deg is hardly affected by operating condition, a significant change is observed at the section near the throat plane. Figure 9 shows the streamlines and the iso-contours of total pressure coefficient ψ in this section at three flow conditions. The magnitudes of ψ are indicated by the grey scale and the flow direction can be identified by the streamlines. It can be seen that the region of high pressure moves towards the cut-off as the flow rate increases and no vortex flow is present in OP 1 and OP 2. It is interesting to note, particularly in the upper casing, the difference in streamline patterns with respect to operating condition. At OP 2, i.e. the best efficiency point, the flow approaches the cut-off almost perpendicularly to the axial axis of the fan rotor whereas at OP 1 and OP 3 it deviates towards the front and back plate of the casing, respectively. Moreover the flow at OP 2 remains relatively uniform as it flows near the cut-off. The deviating streamlines are indicative of the change in the characteristics of the developing limiting streamlines close to the cut-off edge. Therefore at this location the gradients of ψ, particularly the axial component along the rotor axis $\partial\psi/\partial Z$, are affected due to the nature of the flow entering the cut-off clearance. From this plane view the evolution of $\partial\psi/\partial Z$ for the flow approaching the cut-off is consistent with the distributions of C_{pw} on the surface of the casing upstream of the cut-off (c.f. Fig. 6). The comparison of flow patterns between two models does not show any significant difference except that ψ is larger for Model II. Although the location of minimum and maximum values of ψ remains approximately the same between the two models, their magnitude change. For example, the difference in the maximum pressure level $\Delta\psi_{max}$ at OP 1, OP 2 and

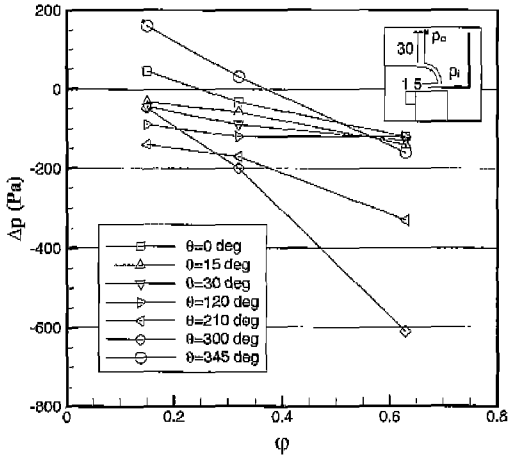

Fig. 10 Differential pressures in the inlet clearance at OP 1, OP 2 and OP 3, for Model I

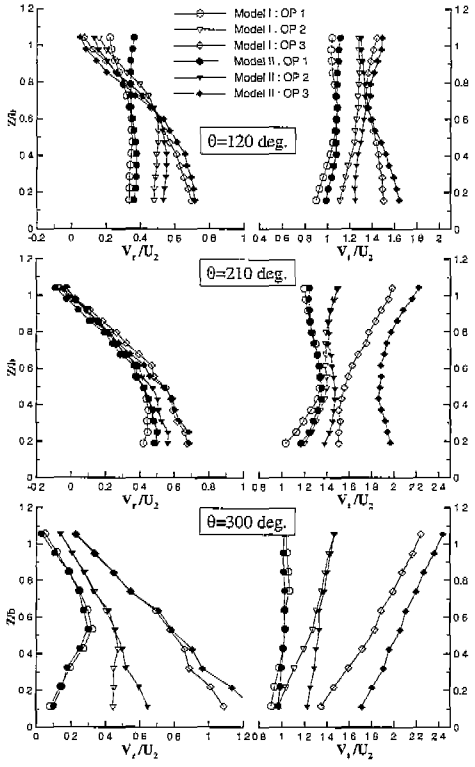

Fig. 11 Spanwise distributions of radial and tangential velocity on the plane $r/D_2=0.58$, at the three operating points

OP 3 is 0.5, 0.3 and 0.7, respectively. This evolution is in accordance with the trends observed in the performance curves (Fig. 4) where the smallest increment of ψ was obtained at OP 2. In contrast to the large value of $\Delta\psi_{max}$ at OP 3 the difference in minimum pressure level $\Delta\psi_{min}$ is remarkably small, i.e. 0.15. This would naturally increase the differential pressure across the fan and may reduce the noise level generated by the vortex flow. Hence, the design improvement of rotor is obtained with Model II. Since the secondary vortex flow generates additional kinetic energy loss together with its mixing characteristics with the primary flow, the mechanical energy of the fluid is lost, so that high rotational speed of the rotor is needed in obtaining high flow capacity particularly in high flow rates. This can explain the rapid decrease of ψ in such flow rates as seen in Fig. 4.

Pressure was also measured in the inlet lip section with a Pitot tube of 0.8mm outer diameter. Figure 10 shows the differential pressure $\Delta p = p_i - p_e$ for various circumferential locations, where p_i and p_e are pressures measured from Pitot tube and static tap, respectively. Their location with respect to the lip is given in Fig. 10. This figure reveals the existence of inlet reverse flow in the vicinity of cut-off. In particular at $\theta_s=345$ deg, the reverse flow or inlet prerotation occurs even at the best efficiency point (OP 2). This agrees with the trends observed by previous computational results in which this phenomenon was apparent in the range between $\theta_s=-20$ deg and $\theta_s=10$ deg (Kwon et al., 2001). Further measurements with a Pitot tube at two different radial positions, $r/D_2=0.454$ and 0.475, were done and showed the same trends as Fig. 10, except in the regions of reverse flow in which the magnitude of Δp reduces as the measurement point r/D_2 increases. An attempt has been made, prior to this measurement, to visualize the reverse flow by introducing smoke into the casing in the proximity of the inlet nozzle lip. Generally the results confirmed measurements; at OP 1, the smoke returning inside the rotor, either through the inlet clearance or the upper portion of the blade channels, was clearly visible near the cut-off region. However at higher flow rates, no reverse flow was apparent over the span of the rotor.

Figure 11 shows the spanwise distributions of the radial and tangential velocity in three circumferential sections, on the plane $r/D_2=0.58$, which is a location in the casing at 11 mm from the rotor exit. The velocities are non-dimensionalized by the rotor tip velocity U_2. The vertical axis is the non-dimensionalized location. Each grouping of symbols (open and filled symbols) means different flow operating condition showing the evolution of radial and tangential component as the flow progresses from low to high flow rate. In all flow conditions the magnitude of the radial velocity V_r is small compared with the tangential velocity V_t. This result is expected given that the V_t is dominant in FC fans with its value greater than U_2. At OP 1 V_r exhibits a relatively flat profile in the upstream location $\theta_s=120$ deg, indicating that the flow leaving the rotor exit is more uniform than in higher flow rates. While the difference in the overall magnitude of V_t remains constant in both models, Model II reveals higher values of V_r than Model I near the shroud region ($Z/b\geq0.8$).

Flow rate variation greatly affects V_r in profile shape and magnitude except in $\theta_s=210$ deg where only a slight difference in magnitude is observed in the lower passage flow ($Z/b\leq0.5$). At circumferential location $\theta_s=210$ deg a local region of negative radial velocity is present in the vicinity of the shroud ($Z/b=1$) at all flow conditions. However, as expected from Fig. 11, its magnitude is small compared with other vector components so that the reverse flow is limited locally within the casing and does not extend to the inlet region. Consequently the reverse flow reenters into the blade channels via the front portion of the rotor inside the casing and generates a loss of guidance from the blades. Therefore the relatively steep gradients of V_r and the presence of reverse flow near the shroud imply a change in flow structure, particularly in secondary flows. In terms of vortex core, its location shifts in the direction of the back plate of the casing resulting in the lowest axial position, as shown in Fig. 8.

As the flow moves further downstream toward $\theta_s=300$ deg, a higher difference in the evolution

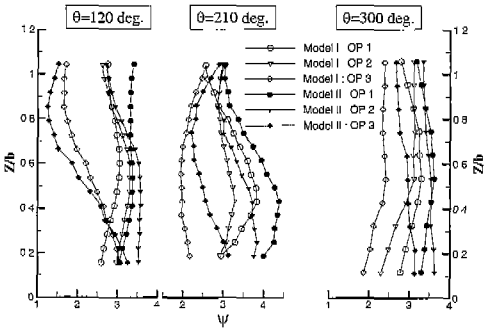

Fig. 12 Spanwise distributions of total pressure coefficient on the plane $r/D_2=0.58$, at the three operating points

of the velocity profiles can be noticed. Throttling to OP 1 causes a considerable reduction in V_r over the lower casing passage flow ($Z/b\leq0.5$) and a constant gradient of V_t profile along the span whereas at higher flow rates, V_r and V_t increase substantially in the region below and above mid-span, respectively. The relatively large difference in velocity profiles with respect to flow rates at downstream locations is evident from previous results (Fig. 9). Model II causes considerable increases both in V_r and V_t over the entire circumference with increasing flow rate. Particularly, a significant change in the lower passage flow is observed as the flow approaches the throat region.

Figure 12 illustrates the spanwise distributions of the total pressure coefficient ψ at $r/D_2=0.58$. High values of ψ mean high magnitude of tangential velocity, both in absolute terms and relative to the other two velocity components, which is indicative of the increase in fan performance. Hence, it can be estimated that the inlet reverse flow, which is generally evident in low and mid flow rates, would be attenuated with Model II. For all operating points this pressure increment generally increases as the flow progresses downstream of the cut-off and tends to be higher in the lower passage flow. Also the flow exhibits less steep gradients and attain a higher overall average increment at the section $\theta_s=300$ deg.

4. Conclusions

Experiments have been performed on two forward-curved centrifugal fans having different geometries. Both rotors were used with the same casing. Even though these fans produce complex flow patterns, the three-dimensional measurements of velocity field have been successfully carried out by using a miniature 5-hole probe.

Regarding the overall fan performance curves higher differential pressure and efficiency are achieved with the new rotor particularly in low flow rates, where aerodynamic unstable phenomena appear. Hence, higher performance and lower noise level are expected with this model. For a given casing, the rotor design is most important for increasing the differential pressure in low and medium flow rates. In high flow rates the casing geometry is expected to play a particularly important role.

The surface flow on the casing near the cut-off exhibited similar behavior in both models, showing a strong axial pressure gradient and higher underpressure level as the flow rate increases. The effect of upstream of the cut-off and FC fan's characteristics having low static pressure and high dynamic pressure at the rotor exit is a possible mechanism to explain this observation. Contrary to what could be expected from literature survey, the secondary flow in the casing didn't protrude the rotor inlet region except near the cut-off where reverse phenomenon occurred up to the best efficiency point. The streamwise component of the velocity within the casing passage was high at all locations. The general flow behavior appeared almost the same for both rotors, although with differences with respect to the location of the vortex core and velocity profiles in the lower casing passage. Especially the radial and streamwise velocity components are increased in the lower casing with the new rotor. Although the flow structure was almost insensitive to operating conditions up to θ_s=300deg, significant differences are obtained near the throat plane indicating the important role of flow characteristics in this region.

References

Bommes, L., Grundmann, R., Klaes, K. and Kramer, C., 1995, "Effects of Blade Design on Centrifugal Fan Noise and Performance," *Noise Control Engineering Journal*, Vol. 43, No. 4, pp. 91~101.

Cau, G., Mandas, N., Manfrida and Nurzia, F., 1987, "Measurements of Primary and Secondary Flows in an Industrial Forward-Curved Centrifugal Fan," *ASME Journal of Fluids Engineering*, Vol. 109, pp. 353~358.

Eck, B., 1973, "Fans," 1st English ed. , Pergamon Press, Oxford.

Fehse, K.-R. and Neise, W., 1999, "Generation Mechanisms of Low-Frequency Centrifugal Fan Noise," *AIAA Journal*, Vol. 37, No. 10, pp. 1173~1179.

Kind, R. J. and Tobin, M. G., 1990, "Flow in a Centrifugal Fan of the Squirrel-Cage Type," *ASME Journal of Turbomachinery*, Vol. 112, pp. 84~90.

Kind, R. J, 1997, "Prediction of Flow Behavior and Performance of Squirrel-Cage Centrifugal Fans Operating at Medium and High Flow Rates," *ASME Journal of Fluids Engineering*, Vol. 119, pp. 639~646.

Koopmann, G. H., Neise, W. and Chen, W., 1988, "Active Noise Control to Reduce the Blade Tone Noise of Centrifugal Fans," *Journal of Vibration, Acoustics, Stress, and Reliability in Design*, Vol. 110, pp. 377~383.

Kwon, E. Y., Baek, K. W., Cho, N. H., Kim, H., K., and Jung, I., J., 2001, "Some Aerodynamic Aspects of Centrifugal Fan Characteristics of an Automotive HVAC Blower," SAE Paper 2001-01-0291, Detroit, USA

Morinushi, K., 1987, "The Influence of Geometric Parameters on F. C. Centrifugal Fan Noise," *Journal of Vibration, Acoustics, Stress, and Reliability in Design*, Vol. 109, pp. 227~234.

Ohta, Y., Outa, E. and Tajima, K., 1996, "Evaluation and Prediction of Blade-Passing Frequency Noise Generated by a Centrifugal Blower," *ASME Journal of Turbomachinery*, Vol. 118, pp. 597~605.

Raj, D. and Swim, W. B., 1981, "Measurements of the Mean Flow Velocity and Velocity Fluctuations at the Exit of an FC Centrifugal Fan Rotor," *ASME Journal of Engineering for Power*, Vol. 103, pp. 393~399.

Roth, H. W., 1981, "Optimierung von Trommelläufer-Ventilatoren," *Strömungsmechanik und Strömungs-maschinen*, Vol. 29, pp. 1~45.

Shepherd, I. C. and Lafontaine, R. F., 1992, "Measurement of Vorticity Noise Sources in a Centrifugal Fan," *Proceedings of the SFA Symposium on Fan Noise*, Senlis, France.

Velarde-Suarez, S., Santolaria-Morros, C. and Ballesteros-Tajadura, R., 1999, "Experimental Study on the Aeroacoustic Behavior of a Forward-Curved Blades Centrifugal Fan," *ASME Journal of Fluids Engineering*, Vol. 121, pp. 276~281.